

# *Drosophila* N-cadherin functions in the first stage of the two-stage layer-selection process of R7 photoreceptor afferents

Chun-Yuan Ting<sup>1,\*</sup>, Shinichi Yonekura<sup>1,\*</sup>, Phoung Chung<sup>1</sup>, Shu-ning Hsu<sup>2</sup>, Hugh M. Robertson<sup>2</sup>, Akira Chiba<sup>2</sup> and Chi-Hon Lee<sup>1,†</sup>

<sup>1</sup>Unit on Neuronal Connectivity, Laboratory of Gene Regulation and Development, National Institute of Child Health and Human Development, National Institutes of Health, Bethesda, MD 20892, USA

<sup>2</sup>Department of Cell and Structure Biology, University of Illinois, Urbana, IL 61801, USA

\*These authors contributed equally to this work

†Author for correspondence (e-mail: leechih@mail.nih.gov)

Accepted 22 December 2004

Development 132, 953–963  
Published by The Company of Biologists 2005  
doi:10.1242/dev.01661

## Summary

Visual information received from the three types of photoreceptor neurons (R1–R6, R7 and R8) in the fly compound eyes converges to the external part of the medulla neuropil (M1–M6 layers) in a layer-specific fashion: R7 and R8 axons terminate at the M6 and M3 layers, respectively, whereas lamina neurons (L1–L5) relay R1–R6 to multiple medulla layers (M1–M5). Here, we show that during development, R7 and R8 neurons establish layer-specific projections in two separate stages: during the first stage, R7 and R8 axons sequentially target to the R7- and R8-temporary layers, respectively; and at the second stage, R7 and R8 growth cones progress synchronously to their destined layers. Using a set of mutations that delete different afferent subsets or alter R7 connectivity, we defined the mechanism of layer selection. We observed that R8, R7 and L1–L5 afferents target to their temporary

layers independently, suggesting that afferent-target, but not afferent-afferent, interactions dictate the targeting specificity. N-cadherin is required in the first stage for R7 growth cones to reach and remain in the R7-temporary layer. The *Ncad* gene contains three pairs of alternatively spliced exons and encodes 12 isoforms. However, expressing a single *Ncad* isoform in *Ncad* mutant R7s is sufficient to rescue mistargeting phenotypes. Furthermore, *Ncad* isoforms mediate promiscuous heterophilic interactions in an in vitro cell-aggregation assay. We propose that *Ncad* isoforms do not form an adhesion code; rather, they provide permissive adhesion between R7 growth cones and their temporary targets.

Key words: *Drosophila*, N-cadherin, R7

## Introduction

Neural circuits of complex brains are frequently organized into parallel layers (laminae), with distinct populations of afferents innervating specific layers (Sanes and Yamagata, 1999). Such layer specificity is widely observed in vertebrate and invertebrate brains, and it probably provides a means to simplify the complexities of synaptic wiring in the central nervous system. Cell-adhesion molecules have been proposed to mediate the interactions of afferents with their synaptic targets during layer selection (Yamagata et al., 2003). In vertebrate retina, the immunoglobulin-superfamily receptors Sidekick 1 and Sidekick 2 specify layer-specific connectivity via their homophilic adhesive activity (Yamagata et al., 2002). Furthermore, the calcium-dependent adhesion receptors, the cadherins, have been proposed to match pre- and postsynaptic partners on the basis of their homophilic binding activity, synaptic localization, and regional and dynamic expression patterns in the brain (Shapiro and Colman, 1999; Yagi and Takeichi, 2000; Iwai et al., 2002). Indeed, antibody-mediated inhibition of N-cadherin caused retinal axons to innervate incorrect layers in chick tectum (Inoue and Sanes, 1997).

The *Drosophila* visual system contains projections from the eye to the brain that segregate in specific layers; the targeting

of these projections is genetically hardwired (Clandinin and Zipursky, 2002; Tayler and Garrity, 2003). It has been used as a model system for studying the development of layer-specific connections. The *Drosophila* compound eye consists of approximately 800 ommatidia, each containing three types of photoreceptor neurons (R1–R6, R7, and R8) (Meinertzhagen and Hanson, 1993). The R1–R6 neurons respond maximally to the blue/green spectrum of light and connect to the first optic neuropil (the lamina), whereas the R7 and R8 are most sensitive to the ultraviolet and blue or green spectra of light, respectively, and connect to the second optic neuropil (the medulla) (Salcedo et al., 1999). The medulla is subdivided into ten layers (M1–M10) based on the terminals of the innervating afferents: the R7 and R8 axons project to the M6 and M3 layers, respectively, while the lamina neurons (L1–5) relay R1–R6 input to multiple medulla layers (Fischbach and Dittrich, 1989).

Genetic screens based on visual behaviors or histology identified three surface receptors, the *Drosophila* N-cadherin (*Ncad*; CadN – FlyBase), the receptor tyrosine phosphatases LAR, and PTP69D, that are required for R7 layer selection (Clandinin et al., 2001; Lee et al., 2001; Maurel-Zaffran et al., 2001; Newsome et al., 2000). N-cadherin and LAR are

required cell-autonomously in the R7 neurons while PTP69D might function in R7 or R8 neurons. Removing N-cadherin or LAR in the R7 neurons results in mutant R7 afferents mistargeting to the R8-recipient layer, and defects in wavelength-discrimination visual behavior. LAR is required for R7 afferents to remain in appropriate target layers during development. The mechanism of action is not known for N-cadherin. The *Drosophila* N-cadherin has a larger complex extracellular domain that mediates homophilic interactions (Iwai et al., 1997). It is evolutionarily conserved in worms, insects, and vertebrates (Broadbent and Pettitt, 2002; Tanabe et al., 2004), and thus may be the most ancient form of classic cadherins. In this study, we investigated the developmental processes of medulla layer formation and the role of N-cadherin therein.

## Materials and methods

### Genetics

Gcm-Gal4 driver (a generous gift from Iris Salecker) is active in lamina precursor cells, and was used to label young L1-L5 axons. For labeling R7s at various developmental stages, the following drivers and genetic schemes were used: PM181-Gal4 driver, which is expressed in R7s prior to axonogenesis, has been described previously (Lee et al., 2001). The relative times of arrival of R7 and L1-L5 axons at the medulla were approximated based on the appearance of the markers in the medulla. UAS-Gal4 (Hassan et al., 2000) was used to extend the activity of PM181-Gal4 for labeling R7 axons at 35% APF (after puparium formation). UAS-mCD8-GFP or UAS-lacZ was used with various Gal4 drivers to label different types of afferents. To label R7 axons beyond 40% APF, we used PM181-Gal4 to drive UAS-Flp. The expression of flipase in R7s removes the interruption cassette in the GMR<interrupt>GFP transgene (a gift from Paul Garrity), and the GMR promoter, in turn, drives the expression of a membrane-tethered GFP (myr-GFP) in the R7s at the late pupal stage. For labeling adult R7s, R7-specific opsin drivers, Rh3-Gal4 and Rh4-Gal4 were used; for adult R8s, R8-specific opsin drivers, Rh5-Gal4 and Rh6-Gal4, were used; for adult L2 cells, L2-Gal4, kindly provided by Andreas Keller, was used; for medulla neurons, Apterous-Gal4 was used.

For genetic cell-ablation experiments, *hh<sup>1</sup>* (eye-specific *hedgheg* allele (Huang and Kunes, 1996), a gift from Sam Kunes), *sev<sup>d2</sup>* (Basler and Hafen, 1989), and UAS-EGFR<sup>DN</sup> were used. To block the differentiation of L1-L5 neurons, we incubated the *Gcm-Gal4* UAS-EGFR<sup>DN</sup> embryos at 17°C to suppress Gal4 activity until they reached the third instar stage. Then, they were moved to a 25°C incubator to allow Gcm-Gal4 to drive the expression of EGFR<sup>DN</sup> in the lamina precursors. The fly stocks were maintained under standard culture conditions at 25°C unless stated otherwise.

The GMR-Flp/MARCM system for generating mosaic R7 neurons has been described (Lee et al., 2001). For analyzing single wild-type or mutant R7s at the 17% and 35% APF, we included the *Elav-Gal4* driver in the genetic scheme. Fly stocks that were used for these experiments are as follows: (1) *GMR-Flp; FRT40*; (2) *GMR-Flp; Ncad<sup>405</sup> FRT40/CyO, ubiP-GFP*; (3) *GMR-Flp; Ncad<sup>B11</sup> FRT40/CyO, ubiP-GFP*; (4) *GMR-Flp; Ncad<sup>M19</sup> FRT40/CyO, ubiP-GFP*; (5) *GMR-Flp; LAR<sup>2127</sup> FRT40/CyO, ubiP-GFP*; (6) *GMR-Flp; Ncad<sup>405</sup> LAR<sup>2127</sup> FRT40/CyO, ubiP-GFP*; (7) *Elav-Gal4<sup>c155</sup>, UAS-mCD8-GFP; tubP-Gal80 FRT40*.

For MARCM rescue experiments, the following stocks were used: (1) *GMR-Flp, UAS-Ncad<sup>7b-13a-18a</sup>, Ncad<sup>405</sup> FRT40/CyO, ubiP-GFP*; (2) *GMR-Flp; Ncad<sup>405</sup> FRT40/CyO, ubiP-GFP; UAS-Ncad<sup>7a-13a-18a</sup>/TM6b*; (3) *GMR-Flp; Ncad<sup>405</sup> FRT40/CyO, ubiP-GFP; UAS-Ncad<sup>7b-13b-18a</sup>/TM6b*; (4) *GMR-Flp; Ncad<sup>405</sup> FRT40/CyO, ubiP-GFP; UAS-Ncad<sup>7b-13a-18b</sup>/TM6b*.

The standard MARCM technique (Lee and Luo, 1999) was used to

generate single-cell clones of L1-L5 and R8 neurons or multiple-cell clones of medulla neurons. Two different heat-shock regimes were used: for generating single-cell lamina clones, 3rd instar larvae were heat-shocked at 37°C for 10 minutes; for medulla neurons or R8s, 2nd instar larvae were heat-shocked at 37°C for 40-60 minutes. The following stocks were used in these experiments: (1) *FRT40*; (2) *Ncad<sup>405</sup> FRT40/CyO, ubiP-GFP*; (3) *Ncad<sup>M19</sup> FRT40/CyO, ubiP-GFP*; (4) *Elav-Gal4<sup>c155</sup>, UAS-mCD8-GFP, hs-Flp; tubP-Gal80 FRT40*.

### Histology

Immunohistochemistry was performed as described previously (Lee et al., 2001). Confocal images were acquired using a Zeiss 510 META laser scanning microscope. The obtained z-stacks of images were deconvolved to remove out-of-focus light and z-distortion with Huygens Professional software (Scientific Volume Imaging) running on a 48 processors SGI Origin 2000. The 3D images were rendered from the restored z-stacks using Imaris software (Bitplane).

### Ncad genomic sequence and transcript analyses

Blast searching using Bioperl scripts (Stajich et al., 2002) and web-based servers was performed to identify potential alternative exons, which were further examined for appropriate splicing donor and acceptor sites. The *Ncad* cDNA corresponding to the 7b-13a-18b isoform (Iwai et al., 1997) was used as query to search against the genomic sequences of *Drosophila melanogaster* (Adams et al., 2000), *Drosophila pseudoobscura*, *Anopheles gambiae* (Holt et al., 2002), and *Apis mellifera*. In addition to the exons 7b, 13a, and 18a reported previously (Iwai et al., 1997), these analyses identified three potential exons corresponding to the exons 7a, 13b, and 18b (Fig. 5).

To obtain experimental evidence for *Ncad* alternative splicing, we analyzed *Ncad* transcripts using RT-PCR. The regions containing potential alternative exons were amplified using the Titan One tube RT-PCR System (Roche), subcloned into the pCR 2.1 vector using the TOPO cloning system (Invitrogen), and sequenced. The obtained cDNA sequences matched the exon sequences predicted from genomic sequence analysis. In addition, a small insertion of 12 bp was found in approximately half of the cDNAs that contain exon 7a. This sequence was further mapped to a small exon, designed 7a', that is located between the common exon 6 and the alternative exon 7a. The sequences of the primers used in RT-PCR are available upon request.

### Molecular biology

The *Ncad* isoform 7b-13a-18a and E-cadherin S2 expression vectors and cDNAs were generous gifts from Tadashi Uemura (Iwai et al., 1997; Oda et al., 1994). The pRmHa3/*Ncad* vectors, for expressing different *Ncad* isoforms in S2 cells, and the pUAS-*Ncad* vectors, for transgene rescue experiments, were constructed as follows. The variable regions corresponding to exons 7a, 13b, 18b were cloned using RT-PCR and confirmed by sequencing. *Ncad* isoform cDNAs were constructed by replacing the variable region in the *Ncad* 7b-13a-18a cDNA. The resulting *Ncad* isoform cDNAs, 7a-13a-18a, 7b-13b-18a, and 7b-13a-18b, were inserted into the S2 expression vector, pRmHa3, or the P-element vector, pUAST. Transgenic flies were generated using standard microinjection techniques.

### Cell-aggregation assay

For expressing different *Ncad* isoforms in suspension S2 cells, different *Ncad* isoform expression vectors (pRmHa3/*Ncad*) were cotransfected with a GFP or Ds-red expression vector (pRmHa3/GFP and pRmHa3/Ds-red). Suspension S2 cells were a generous gift from James Clement (Schmucker et al., 2000). Cell culture and transfection were performed according to the Invitrogen DES and Qiagen Effectene manuals. CuSO<sub>4</sub> was added (0.7 μM) 24 hours after the transfection to induce the expression of *Ncad* isoforms and the GFP or Ds-red marker. The S2 cells were induced for 48 hours and then subjected to cell-aggregation assay as described previously by Oda

(Oda et al., 1994) except for the following modifications. Two populations of S2 cells expressing different cadherins and markers at the concentration  $1.2 \times 10^6$  cell/ml were incubated in 2 ml of the BBS buffer (mM: 10 Hepes, 55 NaCl, 40 KCl, 15 MgSO<sub>4</sub>, 20 glucose, 50 sucrose) containing 5 mM of CaCl<sub>2</sub> in a 35 mm polystyrene dish, and agitated using a gyratory shaker at 100 rpm for 1.5 hours. The formation of cell aggregates was analyzed under a Zeiss M<sup>2</sup>bio fluorescence microscope with a Zeiss AxioCam digital camera. Experiments were performed in triplicates.

### Western blot

Cell lysis and immunoblotting were performed as described (Lee et al., 2001). For each lane, a protein sample equivalent to 200,000 S2 cells was loaded. Rat monoclonal antibody against the cytoplasmic domain of Ncad proteins (Iwai et al., 1997) (a gift from Tadashi Uemura) was used to detect the Ncad proteins.

## Results

### R7 target selection occurs in two distinct stages

To gain insight into the developmental mechanisms governing the formation of layer-specific connections within the medulla, we examined the innervation of medulla by R7, R8, and L1-L5 afferents at various developmental stages. The R-cell growth cones begin to segregate into discrete layers at ~17% pupal formation (17% APF; eclosion at 100%) (Fig. 1A,A'). During this stage, there is a gradient of R7, R8, and L1-L5 growth cones in the medulla neuropil along the anterior-posterior axis, with the newly arriving axons projecting into the anterior edge of the medulla and the older growth cones fully expanded in the posterior edge (Fig. 1A',B',B'). This growth-cone gradient reflects the developmental sequence of the eye discs and the lamina (Fig. 1E, black arrows.)

Superimposed on this temporal gradient is a developmental sequence of the R-cell subtypes and the corresponding lamina neurons (L1-L5). Within each ommatidium, R8 differentiates first, induces the differentiation of the remaining R-cells and L1-L5, and extends its axons into the superficial medulla (R8-temporary layer, Fig. 1A'). The R7s differentiate approximately 24 hours after R8s, and they project axons past the R8 growth cones and terminate at a layer below (R7-temporary layer, Fig. 1A') (Lee et al., 2001). Based on the R7 (PM181-GFP) and L1-L5 (Gcm-LacZ) markers, we estimate that approximately 2–4 hours after the arrival of R7 growth cones at the medulla (corresponding to 1–2 rows), L1-L5 axons reach the medulla and terminate between the R7 and R8 growth cones (Fig. 1B''). The L1-L5 axonal projections in the medulla were further confirmed with the MARCM (mosaic analysis with a repressible cell marker) system (Lee and Luo, 1999), which allowed us to trace single L1-L5 axons (see Fig. S1 in the supplementary material and data not shown). Thus, the layer-specific targeting of R7, L1-L5, and R8 (positioned from proximal to distal layers) at 17% APF does not arise simply from the order of their innervation (R8 first, then R7, and lastly L1-L5), but probably reflects specific properties of different afferents. The distance between R7 and R8 layers increases from ~7  $\mu$ m at 17% APF to ~10  $\mu$ m at 40% APF as the intervening layers further divide into four layers (Fig. 1D') (C.-Y.T. and C.-H.L., unpublished). However, the relative positions of R7, L1-L5, and R8 growth cones (from proximal to distal layers) remain as such until 50% APF, when these growth cones progress to reach their final target layers.

The second stage of R7 and R8 target selection starts at approximately 50% APF. Because the R7-specific Gal4 driver, PM181-Gal4, is inactive at this stage, we used a flipase-based system to label late R7 axons (see Materials and methods). We observed that at this stage the R8 growth cones projected past the L2 growth cones to reach the R7-temporary layer, which later became the R8-recipient layer (Fig. 2B,B'). In addition, the R7 axons extended approximately 3–5  $\mu$ m further into the medulla. During this period, it is possible that as the medulla neuropil continued to develop (see Fig. S2 in the supplementary material), the R-cell growth cones might progress from their temporary layers to their destined layers by processes of active migration and/or passive displacement by the ingrowing medulla processes (or L4-L5 growth cones). By 70% APF, the R7 and R8 growth cones reached their final layers and assumed their adult configurations (Fig. 2D,D'). Thus, layer selection by R7 and R8 axons occurs in two stages. During the first stage, newly differentiating R8 and R7 axons reach their temporary target layers in temporal order according to their time of birth. During the second stage, the R7 and R8 growth cones progress synchronously to their final target layers (Fig. 2H).

### R8, R7, and L1-L5 axons target to distinct medulla layers independently at the first layer-selection stage

Because the projections of L1-L5 axons into the medulla coincide with the separation of the R7 and R8 growth-cone layers, we addressed whether proper medulla lamination requires afferent-afferent interactions, using mutant animals lacking L1-L5 or R7s. In *hh<sup>1</sup>* (an eye-specific allele of *hedgehog*) mutant animals, which lack L1-L5 (Huang and Kunes, 1996; Poeck et al., 2001), we observed that the R7 and R8 growth cones still formed two layers in the medulla although they remained closely associated during the early pupal stage (17% APF; Fig. 3A,A'). To confirm this result with a different approach, we blocked L1-L5 differentiation using Gcm-Gal4 to drive the expression of EGFR<sup>DN</sup>, a dominant negative form of the EGF receptor, in the lamina precursor cells (Huang et al., 1998) (see Materials and methods). This manipulation blocks the differentiation of younger L1-L5 and recapitulated the *hh<sup>1</sup>* phenotype in the younger part of the medulla (bracket in Fig. 3C'). Thus, L1-L5 are not required for the layer selection of R7 and R8 afferents; rather, the L1-L5 growth cones intercalate between the R8 and R7 growth cones to separate them into two distinct layers during the first layer-selection stage (17% APF). Furthermore, in *hh<sup>1</sup>* mutants, the R8 and R7 growth cones segregate into two separate layers at 40% APF (Fig. 3B,B'), presumably due to the extension of intervening dendritic processes of medulla neurons at this stage (C.-Y.T. and C.-H.L., unpublished). Thus, L1-L5 are not specifically required for the separation of the R7 and R8 growth cones.

Conversely, in *sevenless* mutants, which lack R7 neurons (Basler and Hafen, 1989), we observed that L1-L5 and R8 growth cones target to the correct layers (Fig. 3D,D') at 17% APF, indicating that R7s are not required for R8 and L1-L5 axons to reach their temporary target layers. Thus, the interactions between R8, R7, and L1-L5 afferents play only a minor role in medulla layer formation, and afferent-target interaction probably dictates the layer specificity.



### N-cadherin is required for R7 axons to reach and remain in the R7-temporary layer

Using the ultraviolet/visible (UV/Vis) light choice test, we have previously demonstrated that R7 layer selection requires N-cadherin (Lee et al., 2001). To determine the developmental

stage during which *Ncad* functions and to identify the developmental defects in *Ncad* mutant R7s, we modified the single-cell mosaic method previously used for adult phenotypic analysis (GMR-Flp/MARCM), by including the pan-neuronal driver, *Elav-Gal4*. This method allowed us to analyze single

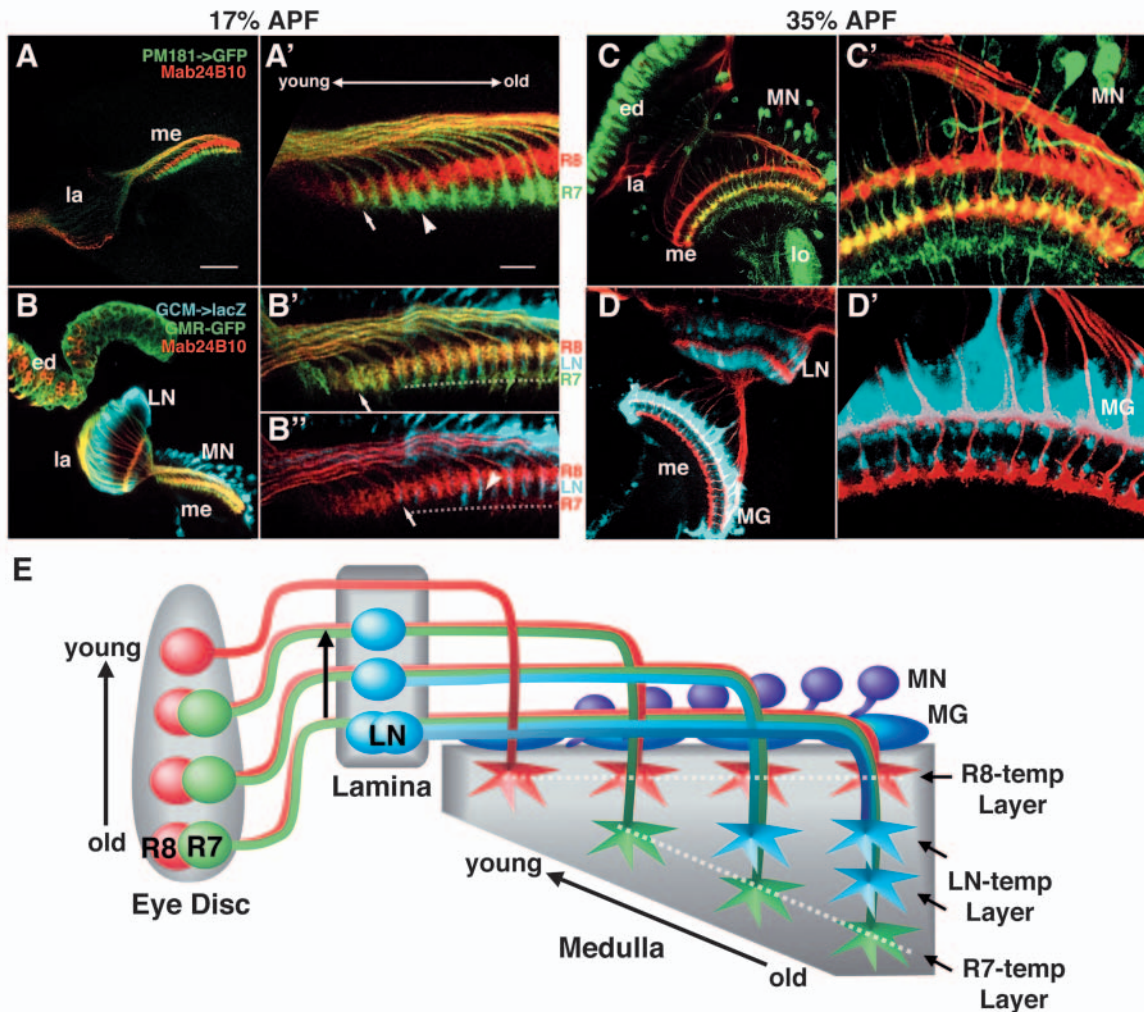


**Fig. 1.** R8, R7, and L1-L5 axons sequentially project into distinct layers in the medulla during the first layer-selection stage. (A,A',B,B',B'') 17% APF; (C,C',D,D',D'') 35% APF. (A,A') The initial projections of R7 and R8 axons were assessed at 17% APF, using PM181-Gal4, UAS-mCD8-GFP (green) and Mab24B10 (red), respectively. (A') A high magnification view of medulla of A. The developing medulla is viewed in cross section to reveal the developmental sequence of R7 and R8 innervation at 17% APF. In this view, the younger R7 and R8 growth cones are to the left and the older ones to the right. The newly arriving R7 growth cones (arrow) project past the R8 growth cones and then expand (arrowhead) to terminate at the layer below the R8 growth cones. (B,B',B'') The L1-L5 projections were viewed in the same direction and at the same stage as in A,A'. The L1-L5 axons expressed *Gcm-Gal4*, UAS-lacZ, and were visualized with anti-lacZ antibody (blue). At this stage, a subset of young medulla neurons (MN) also expresses *Gcm* although their axons have yet to enter the medulla. Both R7 and R8 axons were labeled using a pan-R-cell marker, GMR-GFP (green). R8 axons and older R7 axons are visualized with Mab24B10 (red). (B') A high magnification view of the medulla of B. The newly arriving R7 growth cones (arrow) express GFP but not Mab24B10. (B'') The green channel (GFP) is removed from B' to facilitate the visualization of the L1-L5 projections (blue). Based on the R7 and L1-L5 markers, we estimated that the newly differentiating L1-L5 growth cone (arrow) reaches the medulla ~1-2 rows behind R7s. The older L1-L5 growth cones (arrowhead) terminate between R7 and R8 growth cones. (C,C') R7 and R8 growth cones (red) form two separate medulla layers at 35% APF. R7 axons were labeled using PM181-Gal4, UAS-mCD8-GFP marker, which was prolonged with the UAS-Gal4 method. This method also labels subsets of medulla (MN) and lobular (lo) neurons, which normally express PM181 at a very low level. (D,D') L1-L5 growth cones form two separate layers between R7 and R8 growth cones at 35% APF. The L1-L5 neurons were labeled as in B. At this stage, medulla glia (MG), which wrap around external medulla, express *Gcm*. The presumptive R7-temporary layers are indicated by dotted lines in B',B''. (A'-D') High magnification views of A-D, respectively. ed, eye disc; la, lamina; me, medulla; lo, lobula; LN, L1-L5 neurons; MN, medulla neurons; MG, medulla glia. Scale bars: in A, 30  $\mu$ m for A-D; in A' 10  $\mu$ m for A'-D'. (E) A schematic diagram illustrating the order of R-cell and L1-L5 afferents innervating the medulla. The developmental sequences in the eye disc, lamina, and medulla are indicated by arrows. R8 (red), R7 (green), and L1-L5 (blue) axons sequentially innervate the medulla (gray shaded box) to reach their temporary layers (as indicated).

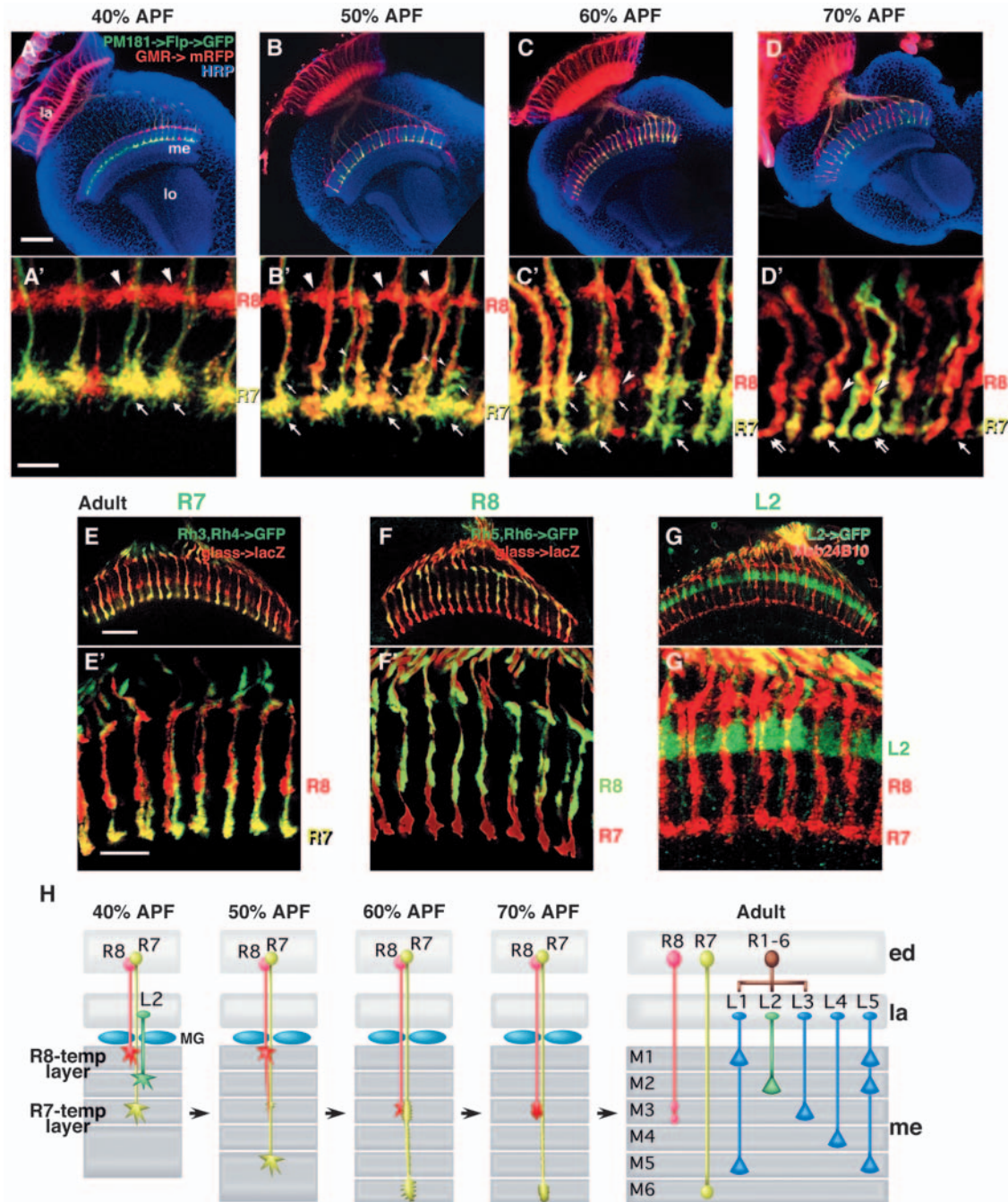


**Fig. 2.** R8 and R7 growth cones reach their destined layers during the second layer-selection stage. (A-D') R7 and R8 layer-specific targeting assessed at 40% (A,A'), 50% (B,B'), 60% (C,C'), and 70% APF (D,D'). Approximately 70% of R7 axons were labeled using a flipase-based method (see Materials and methods) and visualized with the anti-GFP antibody (green). R8 axons (red) were marked with RFP but not GFP. The neuropils were stained with the anti-HRP antibody (purple). (A') At 40% APF, R7 (yellow, large arrow) and R8 (red, large arrowhead) growth cones terminate at their temporary layers. (B') At 50% APF, R7 growth cones (yellow, large arrow) extend ~3  $\mu$ m further with filapodia (small arrow) leaving behind in the R7-temporary layer. R8 growth cones (red) extend filapodia (small arrowhead) deeper into the medulla while leaving their growth cone proper (large arrowhead) in the R8-temporary layer. (C') At 60% APF, both R8 (large arrowhead) and R7 (large arrow) growth cones have reached their final target layers. Note that R7 axon shafts expanded in the R7-temporary layer (small arrow). (D') At 70% APF, both R8 (large arrowhead) and R7 growth cones retract their filapodia and consolidate into axonal terminals. Two types of R7 terminals, straight (large arrow) and horseshoe (double-arrow) are noticeable (as seen in adult flies). (E-G') Layer-specific connections of R7 (C,C'), R8 (D,D') and L2 (E,E') assessed at the adult stage. (E,E') R7 axons (green) were labeled with Rh3 Rh4-Gal4, UAS-synb-GFP. Glass-lacZ marker labeled both R7 and R8 axons (red). (F,F') R8 axons (green) were labeled with Rh5 Rh6-Gal4, UAS-synb-GFP. (G,G') L2 axons (green) were labeled with L2-Gal4 UAS-mCD8-GFP. R7 and R8 axons were visualized with Mab24B10. Note that L2 axons terminate at the M2 layer, just above the R8-recipient layer (M3). (A'-G') High magnification views of A-G, respectively. Scale bars: in A, 30  $\mu$ m for A-D; in A' 5  $\mu$ m for A'-D'; in E, 20  $\mu$ m for E-G; in E', 10  $\mu$ m for E'-G'. (H) A schematic diagram showing the progression of R7 and R8 axonal targeting during the second layer-selection stage. For clarity, most L1-L5 neurons are omitted in the figure for the pupal stages. Abbreviations as in Fig. 1.



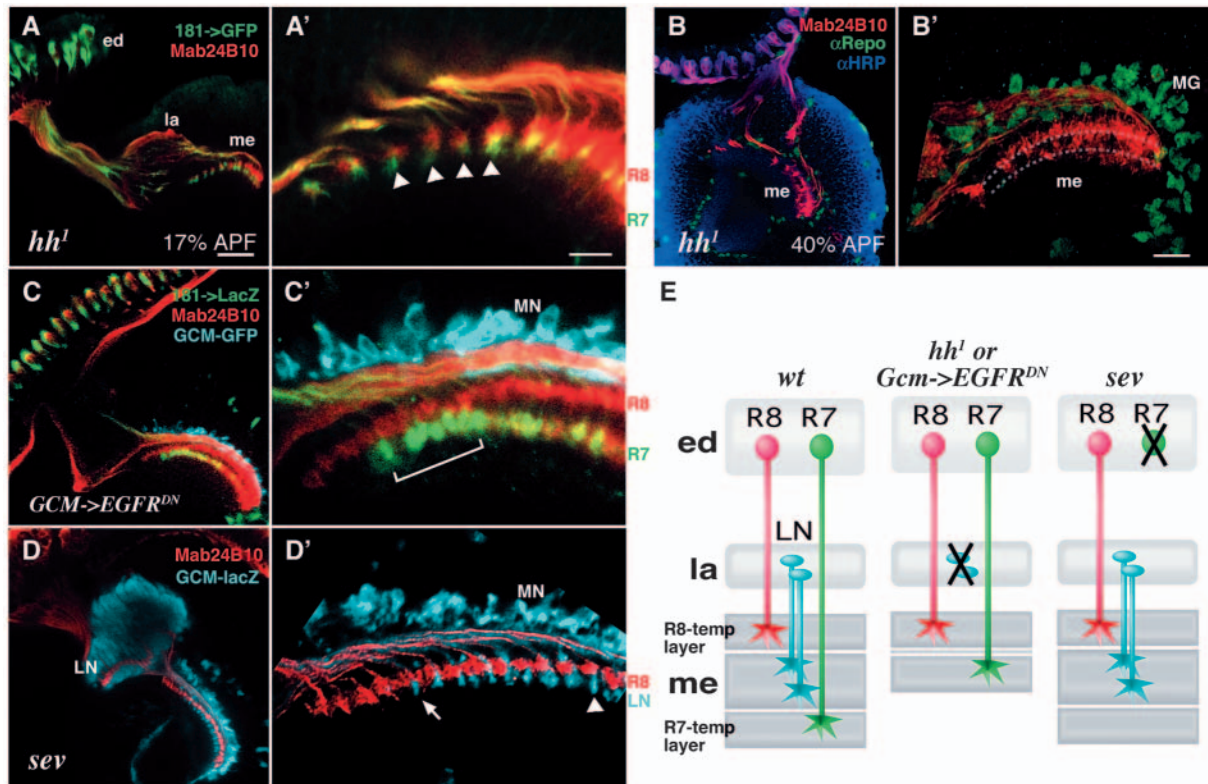


**Fig. 3.** R8, R7, and L1-L5 axons target to distinct medulla layers independently at the first layer-selection stage. (A-D') Layer-specific targeting of R8, R7, and L1-L5 growth cones was assessed in various mutant backgrounds at 17% (A,A',C-D') and 40% APF (B,B'). The R7 axons (green) were labeled using PM181-Gal4, UAS-mCD8-GFP (A,A') or PM181-lacZ marker (C,C'), and visualized with anti-GFP or anti-LacZ antibodies, respectively. The L1-L5 axons (blue) were labeled using Gcm-Gal4, UAS-lacZ and visualized with anti-LacZ antibodies (C-D'). R8 and older R7 axons were visualized with Mab24B10 (red). Glia were visualized with anti-Repo antibody (green in B,B'). (A-B') In *hh'* mutants, L1-L5 fail to differentiate while 11-13 rows of R-cells still develop (Huang and Kunes, 1996). In the absence of L1-L5, the R7 axons project past R8 growth cones and terminate at the layer below (A', arrowheads). However, the R7 growth cones do not separate from R8 growth cones until 40% APF (A,B'). The presumptive R7 and R8 layers were marked with dotted lines. The R-cell growth cones appear disorganized at 40% APF. (C,C') Expressing *EGFR<sup>DN</sup>* in the young lamina blocks the development of L1-L5 in this region and recapitulates the *hh'* phenotypes in the younger part of medulla (bracket). (D,D') In *sevenless* mutants, R7 neurons fail to develop. However, the R8 (red) and L1-L5 (blue) axons (arrow and arrowhead) target correctly to their temporary layers. Scale bars: in A, 30  $\mu$ m for A-D; in A',B', 10  $\mu$ m for A'-D'. (E) A schematic diagram summarizing A,C,D.

wild-type or mutant R7 axons up to 35% APF during which the *Elav* driver is active. We observed that at 17% APF, 21% ( $n=43$ ) of the *Ncad* mutant R7 growth cones failed to reach the R7-temporary layers (Fig. 4B,B'). In addition, many (63%,  $n=43$ ) *Ncad* mutant R7 growth cones exhibited various morphological defects: they failed to expand fully in the medulla, some expanding prematurely before reaching the appropriate layer. We next examined the *Ncad* mutant phenotype at 35% APF, during which the wild-type R7 and R8 growth cones formed two separate layers (Fig. 4E,E'). We observed that 55% ( $n=26$ ) of the *Ncad* mutant R7 axons failed to target to the R7-temporary layer; instead, they terminated at the R8 layer or the layer between the R7 and R8 layers (Fig. 4F,F'). Similar phenotypes and expressivity were observed for three *Ncad* alleles, *Ncad<sup>405</sup>*, *Ncad<sup>M19</sup>*, and *Ncad<sup>b11</sup>* (data not shown). We conclude that at least 24% of the *Ncad* mutant R7 growth cones reach the R7-temporary layer at 17% APF, but retract from the correct layer at 35% APF (results summarized in Fig. 6E).

In contrast, *LAR* mutant R7 axons target correctly at both 17% and 35% APF (arrows, Fig. 4C,C',G,G'), although some mutant growth cones exhibit collapsed morphology

(arrowheads, Fig. 4G'). Using eye-specific mosaic analyses, previous studies showed that the *LAR* mutant R7 growth cones retracted to the R8-temporary layer in the older part of the medulla (Clandinin et al., 2001; Maurel-Zaffran et al., 2001). However, the single-cell mosaic method cannot be used to analyze the older R7 axons because the *Elav-Gal4* driver becomes inactive in these neurons. Removing both *Ncad* and *LAR* in single R7 axons resulted in similar phenotypes to those seen in *Ncad* mutants (Fig. 4D,D',H,H'). In summary, *Ncad*, but not *LAR*, is required for R7 axons to project into the appropriate layer and to remain in the R7-temporary layer at the early pupal stage (17-35% APF).

Because *Ncad* can function as homophilic adhesion molecules in vitro (Iwai et al., 1997) (see below), we next examined whether R7 growth cones use *Ncad* to interact with R8s or medulla neurons, both of which express *Ncad* (Lee et al., 2001). Using the MARCM system, we generated *Ncad* mutant R8 and medulla neuron clones and assessed layer selection in the corresponding R7 growth cones. Removing *Ncad* in single R8 neurons caused R8 growth cones to detach from the R8-temporary layer (62%,  $n=13$ ), but had no effect

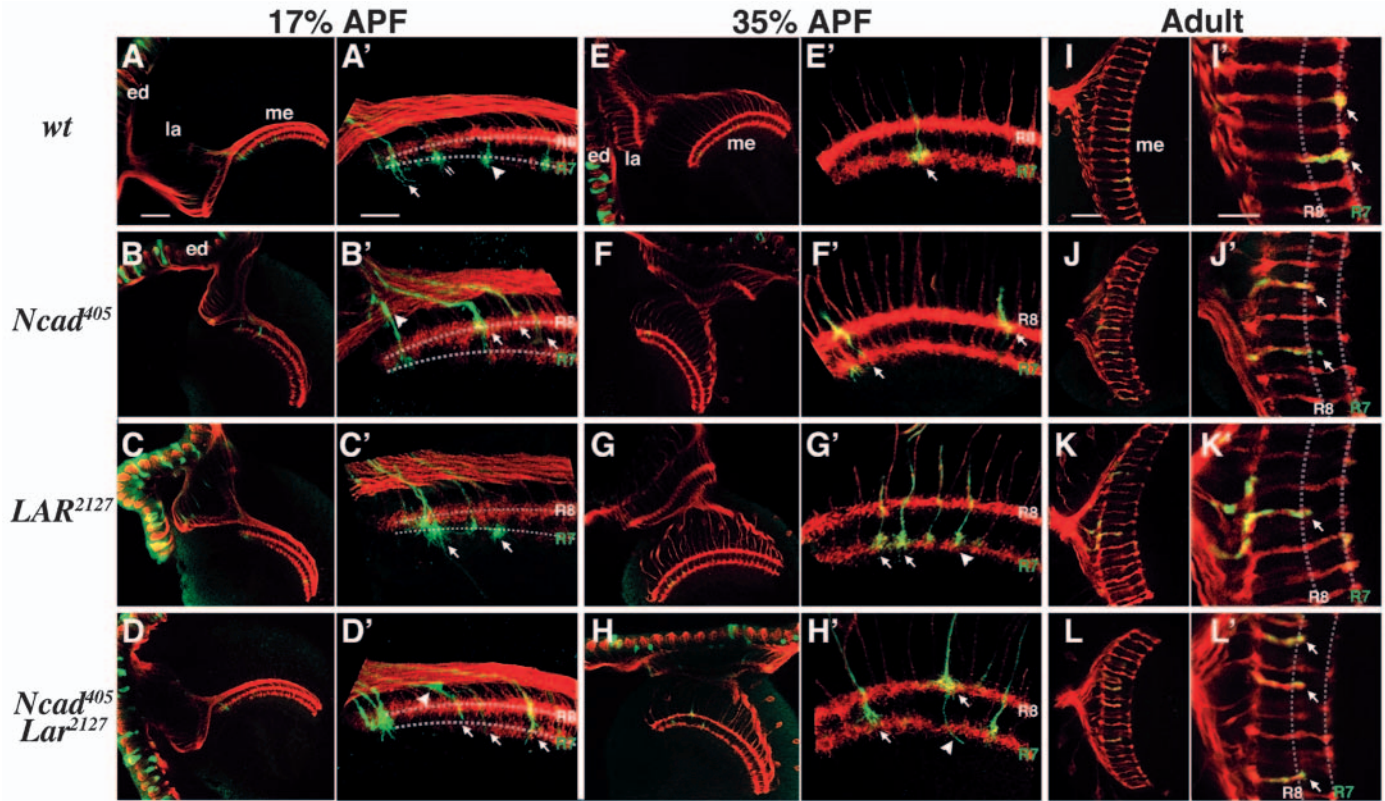


**Fig. 4.** N-cadherin functions in the first layer-selection stage to promote R7 axons reaching and remaining in the R7-temporary layer. R7 targeting was assessed at 17% APF (A–D'), at 35% APF (E–H'), and in adult flies (I–L'). Single mutant R7 cells were generated using GMR-Flp-mediated mitotic recombination (see text), and labeled using the MARCM system and mCD8-GFP (A–H') or synb-GFP (I–L'). R7 and R8 axons were visualized with Mab24B10 (red). (A,A',E,E',I,I') Wild-type; (B,B',F,F',J,J') *Ncad*<sup>405</sup> mutant; (C,C',G,G',K,K') *LAR*<sup>2127</sup> mutant; (D,D',H,H',L,L') *Ncad*<sup>405</sup> *LAR*<sup>2127</sup> double mutant. (A,A') At 17% APF, single R7 cells, homozygous for a wild-type FRT40 chromosome arm, project axons into the medulla. The wild-type axons first project past the R8 layer (arrow), then expand their growth cones (double arrow) just below the R8 growth cones, and separate (arrowhead) from the R8 growth cones. (B,B') At 17% APF, single *Ncad*<sup>405</sup> mutant R7 axons project into the medulla. Approximately 21% of these mutant axons expand their growth cones incorrectly at the R8-temporary layer or between the R7- and R8-temporary layers (arrows). Over half of these mutant growth cones show severe morphological defects (arrowheads). (C,C') Single *LAR*<sup>2127</sup> mutant R7 axons project into the medulla as in wild-type at 17% APF. (D,D') At 17% APF, single *Ncad*<sup>405</sup> *LAR*<sup>2127</sup> double mutant R7 axons exhibit targeting (arrows) and morphological defects (arrowhead) as seen in *Ncad*<sup>405</sup> mutants. (E,E') Single wild-type R7 axons (arrow) terminate at the R7-temporary layer at 35% APF. (F,F') At 35% APF, 55% of the *Ncad* mutant R7 axons (arrow) terminate at the R8-temporary layer or between the R7- and R8-temporary layers. Some of them leave a small filopodium (arrowhead) connecting to the R7-temporary layer. (G,G') At 35% APF, most single *LAR*<sup>2127</sup> mutant R7 axons terminate correctly at the R7-temporary layer in the younger part of the medulla. Approximately 9% of the mutant R7 growth cones exhibit abnormal morphology (arrowhead). Assessment of older R7 axons at this stage is limited because *Elav-Gal4* driver is expressed at a low level in the older R7 cells. (H,H') At 35% APF, single *Ncad*<sup>405</sup> *LAR*<sup>2127</sup> double mutant R7 axons targeted to incorrect layers (arrows), as seen in the *Ncad*<sup>405</sup> mutant. (I,I') In adult flies, single wild-type R7 axons terminate at the R7-recipient layer. (J–L') At the adult stage, single *Ncad*<sup>405</sup> or *LAR*<sup>2127</sup> or *Ncad*<sup>405</sup> *LAR*<sup>2127</sup> double mutant R7 axons terminate incorrectly at the R8-recipient layer. Note that in the region where mutant R7 axons mistarget to the R8-recipient layer, the corresponding R8 axons target correctly to the R8-recipient layer, leaving the R7-recipient layer uninervated by any R-cell afferent. The presumptive R7- and R8-temporary layers are indicated by dotted lines in A'–D', I'–L'. (A'–L') High-magnification views of A–L, respectively. Scale bars: in A, 30  $\mu$ m for A–L; in A', 10  $\mu$ m for A'–L'. Abbreviations as in Fig. 1.

on the corresponding wild-type R7 axons (0%,  $n=13$ ; see Fig. S3A,A' in the supplementary material), indicating that *Ncad* activity is not required in R8s for proper R7 layer selection. Similarly, R7 growth cones targeted correctly to the R7-temporary layer in the presence of small *Ncad* mutant medulla neuron clones (0%, 122 lobes examined; see Fig. S3B–D in the supplementary material). Because of technical difficulty, we were unable to generate large contiguous medulla neuron patches, and, therefore, could not rule out the possibility that *Ncad* would mediate interactions between R7 growth cones and medulla neurons (see Discussion).

#### The *N-cadherin* gene undergoes alternative splicing to generate multiple isoforms

The *Ncad* gene contains three exon modules corresponding to exons 7, 13, and 18, each of which is composed of a pair of highly similar but distinct exons, designated exons 7a/7b, exons 13a/13b, and exons 18a/18b (Fig. 5) (see <http://www.flybase.org/bin/fbidq.html?FBref0141810>). RT-PCR analysis further revealed that mature *Ncad* transcripts contain one and only one of the two alternative exons arising from each exon module (i.e. exon 7a or 7b; 13a or 13b; 18a or 18b), indicating that these exons are used



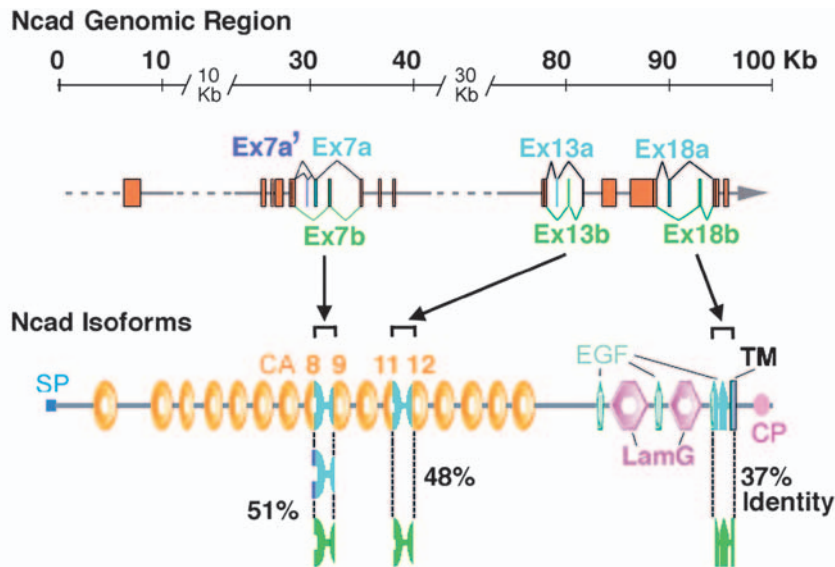


**Fig. 5.** Modular exon organization of the *Ncad* gene. The *Ncad* gene contains 21 exons that span approximately 100 Kb of genomic DNA. Mutually exclusive alternative splicing occurs in exons 7, 13, and 18. As deduced from cDNA sequences, mature mRNA contains exon 7a or 7b, exon 13a or 13b, and exon 18a or 18b. In addition, exon 7a' is found in some exon 7a-containing transcripts. Constant exons are shown as red boxes and alternative exons as green (7a, 13a, 18a) or blue (7b, 13b, 18b) boxes. Exons 7a and 7b each encode the C-terminal half of CA8 and the N-terminal half of CA9; exons 13a and 13b each encode the C-terminal half of CA11 and the N-terminal half of CA12; exons 18a and 18b each encode the C-terminal half of EGF-CA3, the entire EGF-CA4, and the N-terminal half of the TM. The exon 7a' encodes an insertion of four amino-acid residues in CA8. The amino-acid sequence identity between the regions encoded by the alternative exons is indicated. SP: signal peptide; CA: cadherin domain; EGF: EGF-like calcium-binding repeat; LamG: Laminin-G-like domain; TM: transmembrane region; CP: cytoplasmic domain containing  $\beta$ -catenin binding site.

exclusively (data not shown). All six alternative exons were recovered in the RNA isolated from developing eye discs. In addition, we uncovered a small exon, designated as exon 7a', that was found in the exon 7a-containing *Ncad* transcripts, but not in those containing exon 7b. Similar *Ncad* genomic structure was identified in another member of the *Drosophila* family, *D. pseudoobscura*, the malaria mosquito (*Anopheles gambiae*), and, to a lesser extent, the honey bee (*Apis mellifera*) (see Fig. S4 in the supplementary material), all of which diverged from *D. melanogaster*, approximately 55, 250, and 340 million years ago, respectively (Gaunt and Miles, 2002; Tamura et al., 2004). By combinatorial use of these alternative exons, the *Ncad* locus is capable of generating 12 isoforms (encoded by exon 7a, exon 7a+7a', or exon 7b; exon 13a or 13b; exon 18a or 18b). All the *Ncad* alternatively spliced variants share the same domain architecture but have different sequences in the extracellular or the transmembrane regions.

### Expressing single *Ncad* isoforms is sufficient to rescue R7 targeting defects of *Ncad* mutants

Because the developing eye discs express multiple *Ncad* isoforms, we carried out transgene rescue experiments to address whether multiple *Ncad* isoforms are required for R7 targeting. In these experiments, we combined the GMR-

Flp/MARCM system (Lee et al., 2001; Lee et al., 2000) with the UAS-*Ncad* isoform transgene to express a single type of *Ncad* isoform in *Ncad* mutant R7s. We found that expressing a single *Ncad* isoform, including 7a-13a-18a, 7b-13a-18a, 7b-13b-18a, and 7b-13a-18b, substantially, if not completely, rescues the *Ncad* phenotypes in R7 axons (Fig. 6A-E, and data not shown). We found no significant difference in the abilities of different *Ncad* isoform transgenes to rescue the mistargeting or growth cones morphological defects at either 17% or 35% APF (Fig. 6E).

We next sought to determine whether in the wild-type background, mis- or over-expressing a single *Ncad* isoform in R7s alters their target specificity. We used the R7-specific Gal4 driver, PM-181-Gal4, to express *Ncad* isoforms in the wild-type background. We found that expressing any of the isoforms in R7 axons caused modest mistargeting and growth-cone morphological defects (see Fig. S5A',B' in the supplementary material). However, both defects were reduced in the older R7 axons (bracket, see Fig. S5A'',B'' in the supplementary material) and were not observed at the later stage (data not shown). These findings indicate that overexpressing single *Ncad* isoforms in R7 neurons is insufficient to permanently change the R7 target specificity.

### N-cadherin isoforms mediate promiscuous heterophilic interactions

Iwai and colleagues previously reported that the *Ncad* isoform 7b-13a-18a is capable of mediating homophilic interaction in a calcium-dependent manner (Iwai et al., 1997). Because the alternative isoforms differ in the extracellular and transmembrane regions, which could potentially affect the binding specificity, we determined whether the in vitro adhesive activity of *Ncad* isoforms correlates with their indiscriminating activity in R7 layer selection. We modified the S2 cell-aggregation assay to test whether *Ncad* isoforms can mediate heterophilic interaction with one another and with another *Drosophila* classic cadherin, E-cadherin (Oda et al., 1994). Two populations of S2 cells that expressed different types of *Ncad* isoforms were labeled separately with GFP and Ds-Red and mixed using a gyratory shaker under constant rotating speed (see Materials and methods for details). The expression levels of different *Ncad* isoforms were found to be similar (see Fig. S6 in the supplementary material). We found that all tested *Ncad* isoforms induced mixed-cell aggregates, indicating that they can mediate heterophilic interactions (Fig. 7B-E). However, the *Ncad*-expressing S2 cells did not intermix with the S2 cells expressing E-cadherin; instead, they formed separate cell aggregates (Fig. 7A). In summary, the tested *Ncad* isoforms are capable of mediating type-specific heterophilic interactions, but they fail to show any detectable isoform specificity in the in vitro cell-aggregation assays.



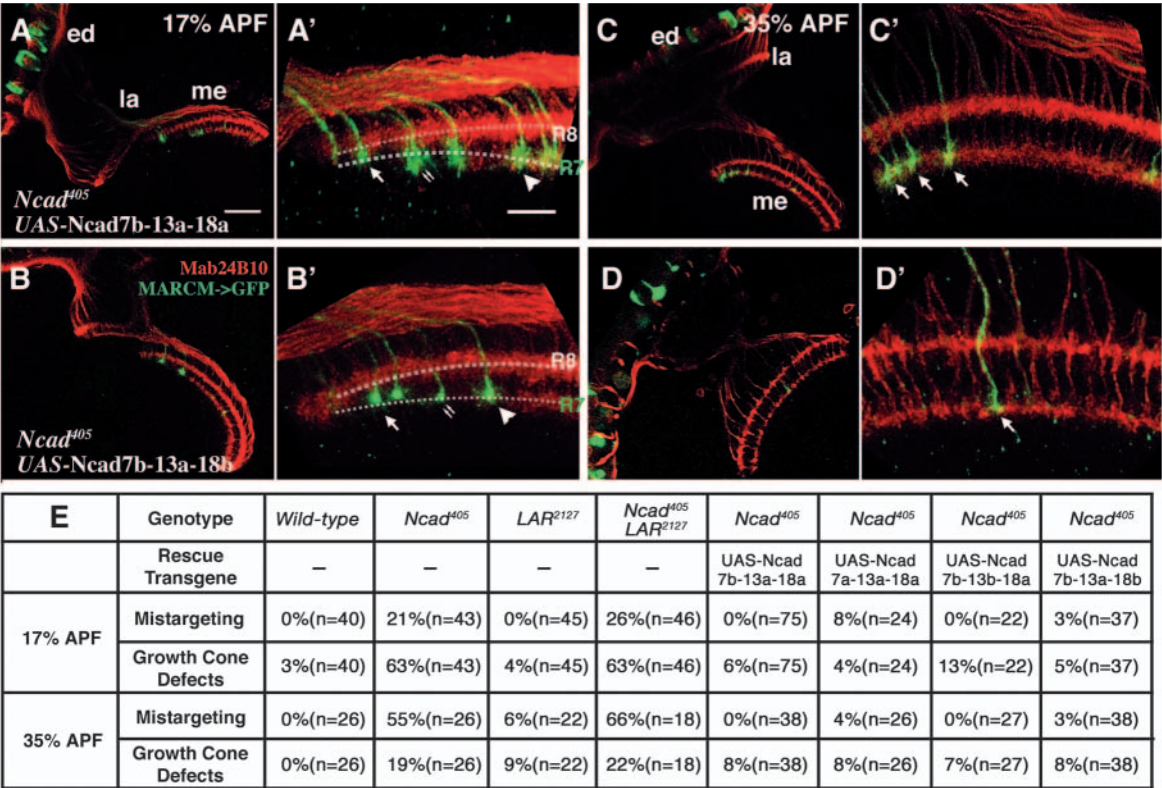


**Fig. 6.** Expressing a single *Ncad* isoform in R7s is sufficient to rescue *Ncad* mutant phenotypes. Single *Ncad* mutant R7 cells were generated using GMR-Flp-mediated mitotic recombination, and a single *Ncad* isoforms 7b-13a-18a (A,A',C,C') or 7b-13a-18b (B,B',D,D') was expressed in these mutant R7s. These R7 axons (green) were labeled using the MARCM system and mCD8-GFP to assess layer-selection at 17% APF (A-B'), and 35% APF (C-D'). As in the wild type, the MARCM-rescued R7 growth cones (arrows) project past the R8-temporary layer and expand their growth cones (double arrows) to terminate (arrowheads) at the R7-temporary layer (A',B') where they still remain at 35% APF (arrows in C',D'). R7 and R8 axons were visualized with Mab24B10 (red). The presumptive R7 and R8-temporary layers are indicated by dotted lines in (A',B'). (A'-D') High-magnification views of A-D, respectively. Scale bars: in A, 30  $\mu$ m for A-D; in A', 10  $\mu$ m for A'-D'. Abbreviations as in Fig. 1. (E) Table summarizing the observed R7 targeting defects in wild type, various mutant backgrounds, and transgene-rescues.

Discussion

In this study, we reveal that R7 layer-specific targeting occurs in two distinct stages: at the first stage, R7 afferents target to the R7-temporary layer where they remain for about one day until the mid-pupal stage (50% APF) when the R7 growth cones progress synchronously to their final target layer. The two-step target selection has been observed in the vertebrate hippocampus: during embryonic development, entorhinal axons and commissural and associational axons form transient synapses with Cajal-Retzius cells and GABAergic interneurons, respectively, before they synapse onto their postnatal targets, the pyramidal neurons (Bayer and Altman, 1987; Super and Soriano, 1998). The two-stage R7 layer selection might serve to coordinate afferent innervation with target development, as in the hippocampus. Alternatively, it might function to reduce the number of potential targets among which R7 growth cones must choose.

Using the mutations that delete different afferent subsets or alter R7 connectivity, we defined the mechanism of R7 layer selection. The genetic cell-ablation results suggest that R8, R7, and L1-L5 afferents target to their temporary layers independently. In addition, the wild-type R8 axons target correctly when the neighboring *Ncad* or *LAR* mutant R7s

mistarget to the R8-recipient layer (Fig. 4J',K'). Conversely, the removal of *Ncad* in single R8s disrupts R8 targeting without affecting the targeting of the neighboring R7s. Thus, the first stage of medulla layer-selection by R8, R7, and L1-L5 afferents probably involves primarily afferent-target interactions. In contrast, R1-R6 growth cone sorting to different lamina cartridges involves both afferent-afferent and afferent-target interactions (Clandinin and Zipursky, 2000; Meinertzhagen and Hanson 1993), even though it required *Ncad* and *LAR* (Lee et al., 2001; Clandinin et al., 2001).

Developmental analyses of single *Ncad* mutant R7s revealed that *Ncad* is required for R7 axons to reach and to remain in the R7-temporary layer during the first layer-selection stage. On the basis of its homophilic activity and mutant phenotypes, we previously proposed that *Ncad* mediates the interaction between the R7 growth cones and the medulla target neurons. The medulla contains over 50 different types of neurons (Fischbach and Dittrich, 1989) and many express *Ncad* during development. It is not technologically feasible at the current stage to remove *Ncad* activity in all or a large number of medulla neurons without affecting the pattern of the optic lobe. Thus, even though we found that removing *Ncad* in small patches of medulla neurons did not affect R7 layer selection,

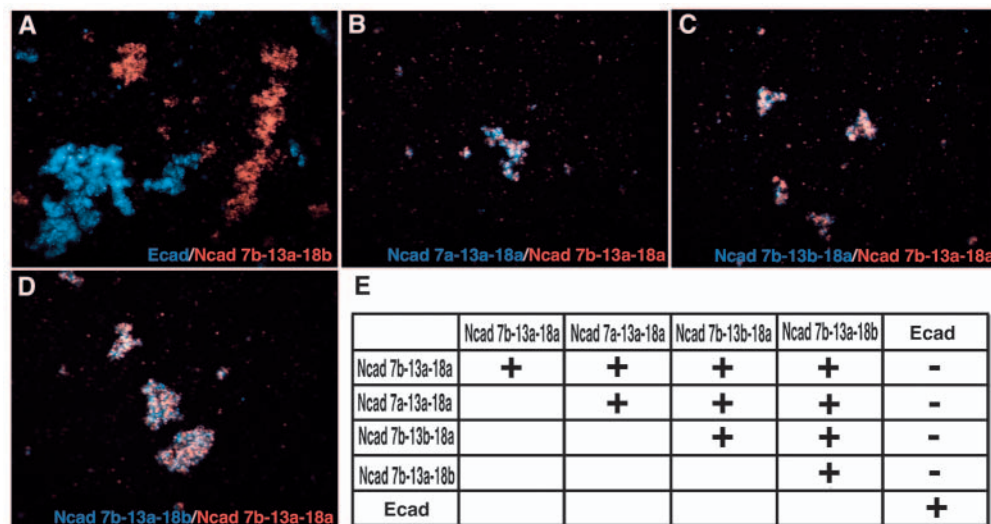


**Fig. 7.** Ncad isoforms mediate promiscuous heterophilic interactions. S2 cells expressing different cadherins and GFP or Ds-red marker are assessed for their ability to induce cell aggregations. (A–D) Cross-adhesion between cells expressing different Ncad isoforms or E-cadherin. Two S2 cell populations expressing different cadherins are separately labeled with GFP (green) or Ds-red (red) and mixed to form aggregates. (A) E-cadherin and Ncad 7b-13a-18b-expressing S2 cells segregate into two types of clusters. (B–D) S2 cells expressing different Ncad isoforms (as indicated) coaggregated to form mixed cell clusters. (E) A table summarizing the cross-adhesion results. +: intermixed; -: segregated.

we cannot rule out the possibility that multiple medulla neurons provide redundant N-cadherin-mediated interactions for R7 growth cones in a similar fashion as L1–L5 neurons do for R1–R6 afferents (S. Prakash and T. Clandinin, personal communication). Alternatively, Ncad might function as a signaling receptor, rather than as a passive adhesive molecule in R7s. Recent studies demonstrated that the cytoplasmic domains of vertebrate classic cadherins could regulate the actin-cytoskeleton via catenins (Yap and Kovacs, 2003). The *Drosophila* Ncad contains the two conserved cytoplasmic regions that interact with catenins in vertebrate cadherins. It is conceivable that Ncad could regulate the actin-cytoskeleton in R7 growth cones in response to target-derived cues. Furthermore, although *Ncad* and *LAR* share the same adult phenotype, their differential onset of mutant phenotype and double mutant phenotype suggest that they probably regulate different aspects of the first R7 layer-selection stage. Ncad is required for R7 growth cones to initially target to, and remain in the R7-temporary layer throughout the first target-selection stage, while *LAR* is only required during the later phase (Clandinin et al., 2001; Maurel-Zaffran et al., 2001).

The comparison between the first and second stages of R7 layer selection reveals a glimpse of the underlying mechanism. First, targeting to the R7-temporary layer at the first stage appears to be critical for the R7 axons to reach their final destination. *Ncad* or *LAR* mutant R7 axons that mistarget to the R8-temporary layer at the first stage, later proceed to terminate incorrectly as well at the R8-recipient layer. Second, in contrast to the initial target selection which follows the axon outgrowth, all R7 and R8 axons enter the second layer-selection stage at approximately the same time, regardless of when they arrive at the medulla. Interestingly, centripetal growth of R1–R6 terminals and synaptogenesis in the lamina coincide with the second stage of R7 layer-selection (Meinertzhagen et al., 2000). It is tempting to speculate that a global signal triggers the initiation of the second stage.

In this study, we report that the *Ncad* gene in *Drosophila*, and probably in other insects, undergoes alternative splicing to generate multiple isoforms. However, the lack of isoform-specificity, revealed by the transgene rescue, overexpression

experiments, and heterophilic interaction assays, argues against the hypothesis that the Ncad isoforms constitute an adhesion code to direct targeting specificity. Instead, we favor the idea that Ncad plays a permissive role in R7 layer selection. Nevertheless, the remarkable conservation of the Ncad alternative splicing over 250 million years of evolution suggests an adaptive advantage for Ncad molecular diversity, whose function awaits further investigation.

We thank Tadashi Uemura, Iris Salecker, Paul Garrity, James Clement, Sam Kunes, and Andreas Keller for providing critical reagents. We thank Benjamin White, Florence Davidson, Alan Hinnebusch, and Henry Levin for carefully reading the manuscript and helpful discussions, Keita Koizumi for generating transgenic flies, Kimberly Hung for cloning *Ncad* cDNA, and Larry Zipursky and Thomas Clandinin for communicating results prior to publication. We thank Catherine Malo and Margaret Dieringer for manuscript handling and editing. This work is supported by the NIH grant HD008748-03 to C.H.L.; S.Y. is a fellow of the Japan Society for the Promotion of Science.

### Supplementary material

Supplementary material for this article is available at <http://dev.biologists.org/cgi/content/full/132/5/953/DC1>

### References

- Adams, M. D., Celniker, S. E., Holt, R. A., Evans, C. A., Gocayne, J. D., Amanatides, P. G., Scherer, S. E., Li, P. W., Hoskins, R. A., Galle, R. F. et al. (2000). The genome sequence of *Drosophila melanogaster*. *Science* **287**, 2185–2195.
- Basler, K. and Hafen, E. (1989). Dynamics of *Drosophila* eye development and temporal requirements of sevenless expression. *Development* **7**, 723–731.
- Bayer, S. A. and Altman, J. (1987). Directions in neurogenetic gradients and patterns of anatomical connections in the telencephalon. *Prog. Neurobiol.* **29**, 57–106.
- Broadbent, I. D. and Pettitt, J. (2002). The *C. elegans* hmr-1 gene can encode a neuronal classic cadherin involved in the regulation of axon fasciculation. *Curr. Biol.* **12**, 59–63.
- Clandinin, T. R. and Zipursky, S. L. (2000). Afferent growth cone interactions control synaptic specificity in the *Drosophila* visual system. *Neuron* **28**, 427–436.
- Clandinin, T. R. and Zipursky, S. L. (2002). Making connections in the fly visual system. *Neuron* **35**, 827–841.
- Clandinin, T. R., Lee, C. H., Herman, T., Lee, R. C., Yang, A. Y.,



- Ovasapyan, S. and Zipursky, S. L. (2001). *Drosophila* LAR regulates R1-R6 and R7 target specificity in the visual system. *Neuron* **32**, 237-248.
- Fischbach, K. F. and Dittrich, A. P. (1989). The optic lobe of *Drosophila melanogaster*. I. A golgi analysis of wild-type structure. *Cell Tissue Res.* **258**, 441-475.
- Gaunt, M. W. and Miles, M. A. (2002). An insect molecular clock dates the origin of the insects and accords with palaeontological and biogeographic landmarks. *Mol. Biol. Evol.* **19**, 748-761.
- Hassan, B., Bermingham, N., He, Y., Sun, Y., Jan, Y., Zoghbi, H. and Bellen, H. (2000). atonal regulates neurite arborization but does not act as a proneural gene in the *Drosophila* brain. *Neuron* **25**, 49-61.
- Holt, R. A., Subramanian, G. M., Halpern, A., Sutton, G. G., Charlab, R., Nusskern, D. R., Wincker, P., Clark, A. G., Ribeiro, J. M., Wides, R. et al. (2002). The genome sequence of the malaria mosquito. *Science* **298**, 129-149.
- Huang, Z. and Kunes, S. (1996). Hedgehog, transmitted along retinal axons, developing visual centers of the *Drosophila*. *Cell* **86**, 411-422.
- Huang, Z., Shilo, B. Z. and Kunes, S. (1998). A retinal axon fascicle uses spitz, an EGF synaptic cartridge in the brain of *Drosophila*. *Cell* **95**, 693-703.
- Inoue, A. and Sanes, J. R. (1997). Lamina-specific connectivity in the brain: neurotrophins, and glycoconjugates. *Science* **276**, 1428-1431.
- Iwai, Y., Usui, T., Hirano, S., Steward, R., Takeichi, M. and Uemura, T. (1997). Axon patterning requires DN-cadherin, a novel in the *Drosophila* embryonic CNS. *Neuron* **19**, 77-89.
- Iwai, Y., Hirota, Y., Okano, H., Takeichi, M. and Uemura, T. (2002). DN-cadherin is required for spatial arrangement of nerve terminals and ultrastructural organization of synapses. *Mol. Cell. Neurosci.* **19**, 375-388.
- Lee, C. H., Herman, T., Clandinin, T. R., Lee, R. and Zipursky, S. L. (2001). N-cadherin regulates target specificity in the *Drosophila* visual system. *Neuron* **30**, 437-450.
- Lee, T. and Luo, L. (1999). Mosaic analysis with a repressible cell marker function in neuronal morphogenesis. *Neuron* **22**, 451-461.
- Lee, T., Marticke, S., Sung, C., Robinow, S. and Luo, L. (2000). Cell-autonomous requirement of the USP/EcR-B mushroom body neuronal remodeling in *Drosophila*. *Neuron* **28**, 807-818.
- Maurel-Zaffran, C., Suzuki, T., Gahmon, G., Treisman, J. E. and Dickson, B. J. (2001). Cell-autonomous and -nonautonomous functions of LAR in R7 photoreceptor axon targeting. *Neuron* **32**, 225-235.
- Meinertzhagen, I. A. and Hanson, T. E. (1993). The development of the optic lobe. In *The Development of Drosophila melanogaster*, vol. 2, pp. 1363-1491. Cold Spring Harbor, NY: Cold Spring Harbor Laboratory Press.
- Newsome, T. P., Asling, B. and Dickson, B. J. (2000). Analysis of *Drosophila* photoreceptor axon guidance in eye-specific mosaics. *Development* **127**, 851-860.
- Meinertzhagen, I. A., Piper, S. T., Sun, X.J. and Frohlich, A. (2000). Neurite morphogenesis of identified visual interneurons and its relationship to photoreceptor synaptogenesis in the flies, *Musca domestica* and *Drosophila melanogaster*. *Eur. J. Neurosci.* **12**, 1342-1356.
- Oda, H., Uemura, T., Harada, Y., Iwai, Y. and Takeichi, M. (1994). A *Drosophila* homolog of cadherin associated with armadillo and essential for embryonic cell-cell adhesion. *Dev. Biol.* **165**, 716-726.
- Pertz, O., Bozic, D., Koch, A. W., Fauser, C., Brancaccio, A. and Engel, J. (1999). A new crystal structure, Ca<sup>2+</sup> dependence and mutational analysis reveal molecular details of E-cadherin homoassociation. *EMBO J.* **18**, 1738-1747.
- Poeck, B., Fischer, S., Gunning, D., Zipursky, S. L. and Salecker, I. (2001). Glial cells mediate target layer selection of retinal axons in the developing visual system of *Drosophila*. *Neuron* **29**, 99-113.
- Salcedo, E., Huber, A., Henrich, S., Chadwell, L. V., Chou, W. H., Paulsen, R. and Britt, S. G. (1999). Blue- and green-absorbing visual pigments of *Drosophila*: ectopic expression and physiological characterization of the R8 photoreceptor cell-specific Rh5 and Rh6 rhodopsins. *J. Neurosci.* **15**, 10716-10726.
- Sanes, J. R. and Yamagata, M. (1999). Formation of lamina-specific synaptic connections. *Curr. Opin. Neurobiol.* **9**, 79-87.
- Schmucker, D., Clemens, J. C., Shu, H., Worby, C. A., Xiao, J., Muda, M., Dixon, J. E. and Zipursky, S. L. (2000). *Drosophila* Dscam is an axon guidance receptor exhibiting extraordinary molecular diversity. *Cell* **101**, 671-684.
- Shapiro, L. and Colman, D. R. (1999). The diversity of cadherins and implications for a synaptic adhesive code in the CNS. *Neuron* **23**, 427-430.
- Stajich, J., Block, D., Boulez, K., Brenner, S., Chervitz, S., Dagdigan, C., Fuellen, G., Gilbert, J., Korf, I., Lapp, H. et al. (2002). The Bioperl toolkit: perl modules for the life sciences. *Genome Res.* **12**, 1611-1618.
- Super, H. and Soriano, E. (1998). Involvement of distinct pioneer neurons in the formation of layer-specific connections in the hippocampus. *J. Neurosci.* **18**, 4616-4626.
- Tamura, K., Shan, W. S., Hendrickson, W. A., Colman, D. R. and Shapiro, L. (1998). Structure-function analysis of cell adhesion by neural (N-) cadherin. *Neuron* **20**, 1153-1163.
- Tamura, K., Subramanian, S. and Kumar, S. (2004). Temporal patterns of fruit fly (*Drosophila*) evolution revealed by mutation clocks. *Mol. Biol. Evol.* **21**, 36-44.
- Tanabe, K., Takeichi, M. and Nakagawa, S. (2004). Identification of a nonchordate-type classic cadherin in vertebrates: chicken Hz-cadherin is expressed in horizontal cells of the neural retina and contains a nonchordate-specific domain complex. *Dev. Dyn.* **229**, 899-906.
- Taylor, T. and Garrity, P. (2003). Axon targeting in the *Drosophila* visual system. *Curr. Opin. Neurobiol.* **13**, 90-95.
- Yagi, T. and Takeichi, M. (2000). Cadherin superfamily genes: functions, genomic organization, and neurologic diversity. *Genes Dev.* **14**, 1169-1180.
- Yamagata, M., Sanes, J. R. and Weiner, J. A. (2003). Synaptic adhesion molecules. *Curr. Opin. Cell Biol.* **15**, 621-632.
- Yamagata, M., Weiner, J. A. and Sanes, J. R. (2002). Sidekicks: synaptic adhesion molecules that promote lamina-specific connectivity in the retina. *Cell* **110**, 649-660.
- Yap, A. S. and Kovacs, E. M. (2003). Direct cadherin-activated cell signaling: a view from the plasma membrane. *J. Cell Biol.* **160**, 11-16.